CHEMISTRY OF MATERIALS

pubs.acs.org/cm

Article

Lanthanide Borocarbides $Ln_3BC_2X_n$ (Ln = La−Pr; X = H, F, Cl) Grown from Metal Flux: From Magnetic Ordering to Superconductivity

Published as part of Chemistry of Materials special issue "In Memory of Prof. Francis DiSalvo".

James T. Larson, Katelyn Wix, Olatunde Oladehin, Ryan Baumbach, Xiaoping Wang, and Susan E. Latturner*

Cite This: https://doi.org/10.1021/acs.chemmater.4c02111

Read Online

ABSTRACT: New stuffed lanthanide borocarbides were grown from reactions in lanthanide-rich eutectic melts, exploring the use of $C_{14}H_{10}$ (anthracene), $C_{12}F_{10}$ (decafluorobiphenyl), and $LnCl_3$ as sources of interstitial hydride, fluoride, and chloride ions. $Ln_3BC_2X_n$ (Ln = La, Ce, Pr; X = H, F) are analogues of the orthorhombic $Ca_3C_3Cl_2$ structure type, featuring borocarbide units in place of the allenylide anions and small anions (X = H and F) in place of the chloride anions, partially occupying octahedral and tetrahedral interstitial sites surrounded by lanthanide cations. Single-crystal neutron diffraction data for $La_3BC_2H_{1.69}$ confirm that hydrogen is present in both interstitial sites, with site-splitting in the octahedral site. Magnetic studies and resistivity measurements indicate that $La_3BC_2H_{1.69}$ shows superconductivity with a T_c near 4.5 K. $Pr_3BC_2H_x$ shows ferromagnetic ordering below 55 K, while the fluoride analogue $Pr_3BC_2F_{0.71}$ is paramagnetic. Attempts to incorporate chlorine into the interstitial sites lead to a structure change to the $La_3BC_2Br_2$ structure type.

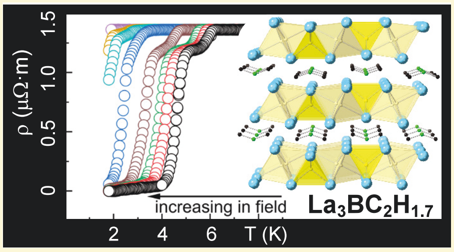

■ INTRODUCTION

Intermetallics are compounds composed of two or more metals or metalloids that have their own distinct crystallographic sites in the structure. Many intermetallic compounds have interesting magnetic and electronic behavior as well as many useful mechanical properties.[1] This leads to applications from computer hard drives and electric motors ($Nd_2Fe_{14}B$) to aerospace and automotive materials (TiAl turbocharger turbines).[2,3] Many intermetallics are also superconductors (RNi_2B_2C and MgB_2).[4,5] Magnetic and electronic properties of intermetallic compounds can be modified by the addition of interstitial atoms, such as carbon, boron, and hydrogen. For example, Buschow and Sherwood found that YMn_2, $LuMn_2$, and $ThMn_{23}$ varied between Pauli paramagnetic and ferromagnetic behavior after the absorption of hydrogen due to the resulting change in lattice parameters, which increased the Mn−Mn separation.[6] Interest in the interaction of hydrogen with lanthanide metals has been further driven by the recent discovery of superconductivity in the high-pressure phase LaH_{10}, which has a T_C of 250 K.[7]

Synthesis of intermetallic compounds (especially metal carbides and borides) is usually carried out at high temperatures, requiring the use of arc-melting, RF-induction heating, or lengthy furnace annealing. This is because the reactants used are refractory solids and must be melted for the reaction to proceed; alternately, the reaction may occur via slow solid-state diffusion across grain boundaries. Because of the high temperatures required, these reactions typically yield the most thermodynamically stable products, which are often simple binary or ternary compounds.[8,9] This method can also lead to polycrystalline ingots containing several byproducts or secondary phases. This is particularly problematic for superconductors, as demonstrated by the reports on superconductivity in "$La_5B_2C_6$" at 7 K, which was later found to be due to the presence of the $La_2C_{3-x}B_x$ contaminant.[10,11]

Metal flux synthesis has been extensively explored as an alternative low-temperature method to form intermetallics. Flux reactions use low melting metals or eutectic mixtures as solvents for the dissolution of elements and the formation of intermetallic products. The lower temperatures of metal flux synthesis allow for more complex intermetallics to be grown.[8,9] Because it is a solution method, metal flux synthesis also enables the growth of crystals, which ensures phase purity of samples and facilitates characterization. Lanthanide-rich eutectic mixtures have proven to be fruitful reaction media for the synthesis of lanthanide intermetallics, exemplified by the growth of $Ce_{21}Fe_8Sn_7C_{12}$ (from Ce/Ni flux), $Pr_{14}Fe_6C_{13}$ (from Pr/Ni flux), and $La_{33}Fe_{14-x}Al_{x+y}B_{25-y}C_{34}$ (from La/Ni flux).[12−14] We have recently found that hydrocarbons react in

Received: July 28, 2024
Revised: September 23, 2024
Accepted: September 24, 2024

Ln/T fluxes to act as a source of carbon and hydrogen, yielding products such as $La_{15}(FeC_6)_4H$ and $Ce_4B_2C_2H_{2.4}$, and that fluorinated analogues can be made by using fluorocarbon reactants.[15−18]

In this work, we report the metal flux synthesis of a new family of borocarbide compounds with an orthorhombic structure related to that of $Ca_3C_3Cl_2$.[19] Boron is reacted with a carbon source and an interstitial anion source in lanthanide-rich eutectic melts. The resulting $Ln_3BC_2X_n$ (Ln = La, Ce, Pr; X = H, F, Cl) products contain borocarbide chains surrounded by lanthanide cations. Anionic species incorporate between layers of lanthanide cations. The presence of hydride in $La_3BC_2H_{1.69}$ is confirmed by neutron diffraction; magnetic susceptibility and resistivity measurements indicate that this compound is a superconductor. The magnetic behavior of the Pr analogues depends on the identity of the interstitial element. Attempts to incorporate a larger interstitial species (chloride) lead to a structure change. This new $Ln_3BC_2X_n$ family of compounds represents a highly tunable platform for the investigation of superconductivity and magnetism, given the variation that is possible for the identity and occupancy of the interstitial atoms X, as well as the lanthanide element.

■ EXPERIMENTAL PROCEDURE

Synthesis. $Ce_3BC_2H_x$ was initially discovered as a low-yield product in a reaction of 1 mmol of boron (99.4% Strem Chemicals, powder, crystalline) and 1 mmol of carbon (99.99% Strem Chemicals, acetylene carbon black, powder) with 2.6 mmol of copper (99.5% Alfa Aesar, powder, −40 + 100 mesh) and 7.4 mmol of cerium (99.9% REO Strem Chemicals, ingot). These reactants were placed in an alumina crucible with the boron being loaded first, followed by carbon, then copper, and cerium being loaded on top. As the lowest melting reactant, the cerium melts and flows onto the copper to produce a Ce/Cu melt in situ, which then dissolves the other reactants. The filled crucible was then placed in a fused-silica sleeve with a wad of Fiberfrax above the alumina crucible, which was then attached to a vacuum line, evacuated to below 100 mTorr, and flame-sealed. The sealed ampule was placed into a furnace and heated to 1000 °C for 3 h, held at that temperature for 6 h, cooled to 850 °C over the course of 24 h and maintained at that temperature for 18 h, and then gradually cooled to 550 °C over the course of 96 h. Once the reaction cooled to 550 °C, it was then taken out of the furnace, inverted, and centrifuged to separate the molten flux from the products.

Because the $Ce_3BC_2H_x$ product was found to have the $Ca_3C_3Cl_2$ structure type, it was hypothesized that hydrogen was occupying the empty chloride sites (vide infra). The cerium was used as received and was presumably the source of the hydride contaminant; this has been previously seen to introduce adventitious hydrogen to intermetallic compounds.[16] After the product was initially characterized, subsequent reactions were carried out using prealloyed Ln/Ni eutectics with ratios of La/Ni (88:12 wt %), Ce/Ni (92:8 wt %), and Pr/Ni (88:12 wt %) that melt at 532, 560, and 525 °C, respectively. These eutectics were made by arc-melting the specific ratios of the two metals in an argon environment after a separate zirconium getter slug was melted to eliminate oxide contamination. The resulting Ln/Ni ingots were flipped and remelted several times to ensure homogeneity.

Because this arc-melting process would remove adventitious hydrogen through thermal decomposition of any hydride or hydroxide present in the lanthanide metals, the subsequent reactions included anthracene ($C_{14}H_{10}$, Sigma-Aldrich 97%), acting as both a carbon and hydride source. The reactions were prepared by loading anthracene, then boron, and then pieces of the prealloyed Ln/Ni fluxes into an alumina crucible. The crucible was sealed in a quartz tube under a vacuum as described above. The reactions were heated to 950 °C for 3 h, held at 950 °C for 12 h, and cooled to 600 °C in 120 h. It was found that annealing the reaction at this temperature for 84 h led to the growth of larger crystals. After being annealed, the ampules were removed from the furnace, inverted, and centrifuged to separate the crystallized products from the excess flux melt.

To explore the incorporation of fluoride interstitials, decafluorobiphenyl ($C_{12}F_{10}$, TCI 98.0%) was used as a source of both carbon and fluorine. It was found that $C_{12}F_{10}$ had to be kept separate from the rest of the reactants to avoid formation of ionic metal fluorides. This was achieved by placing the $C_{12}F_{10}$ powder directly into the quartz tube first; the rest of the reactants (boron and pieces of prealloyed Ln/Ni flux) were loaded into an alumina crucible, which was then placed into the quartz tube on top of the $C_{12}F_{10}$. The quartz tube was chilled in an ice bath for 5 min before being sealed under vacuum to keep the $C_{12}F_{10}$ from volatilizing during the flame-sealing process. The same heating profile was used as described above.

The chloride compounds ($La_3BC_2Cl_x$) were grown by reacting carbon (acetylene carbon black, 99.99% Strem Chemicals), boron (crystalline powder, 99.4% Strem Chemicals), and $LaCl_3$ (99.9% Strem Chemicals) in 90:10 mol % La/Fe flux. The lanthanum pieces are from BeanTown Chemical (99.9%), and the iron powder is from Macron (100 mesh). This La/Fe mixture has a melting point of 800 °C. Reactions were run in alumina crucibles, with 0.55 mmol of $LaCl_3$ placed at the bottom of the crucible, then 1 mmol of B placed on top of it, 2 mmol of C, 1.15 mmol of Fe, and 10.23 mmol of La placed in the crucible last. The La pieces were stored under mineral oil, so they were washed with hexanes before being placed in the crucible. La was placed on top of the Fe because La will melt first at 918 °C, melting down onto the Fe, making a flux mixture. The loaded crucibles were placed in a quartz tube. A wad of Fiberfrax was placed in the tube above the crucible; the tubes were then flame-sealed under a vacuum and placed in a programmable furnace. The reactions were heated to 1100 °C for 3 h, held at that temperature for 12 h, and gradually cooled to 830 °C over the course of 60 h, at which point they were removed from the furnace and centrifuged to remove the excess flux.

Caution: The thermal decomposition of $C_{14}H_{10}$ and $C_{12}F_{10}$ generates gaseous pressure in the sealed ampules during heating. To avoid rupture of the ampules (which have 1.1 cm internal diameter and are roughly 10 cm long, with a total volume of 9−10 cm^3), small amounts (less than 0.4 mmol) of the volatile compounds must be used. Gloves, eye protection, and face shields were used during removal of the ampules from the furnace and when placing them in the centrifuge. The cooled ampules were wrapped in foil before breaking them open to contain any glass shards. All $Ln_3BC_2X_n$ compounds are air-sensitive and must be stored under nitrogen.

Elemental Analysis. Elemental analysis was done using an FEI NOVA 400 scanning electron microscope equipped with energy-dispersive X-ray spectroscopy (SEM-EDS). Crystals were selected under an optical microscope and positioned on an aluminum puck by using double-sided carbon tape. To eliminate spurious readings from flux residue on the surface, each crystal was cleaved and arranged on the carbon tape, so that the inside surface was perpendicular to the electron beam. An acceleration voltage of 30 kV was used. EDS data for all $Ln_3BC_2X_n$ compounds confirmed the presence of the lanthanide elements as well as boron and carbon; however, the amount of boron and carbon cannot be quantitatively determined due to the insensitivity of this method to light elements. The characteristic X-ray peak for fluorine (at 0.68 keV) was observed in crystals from reactions with decafluorobiphenyl; similarly, the chlorine peak (at 2.61 keV) was observed for $La_3BC_2Cl_x$ products. Incorporation of the transition metal from the flux or aluminum from the crucible was not observed.

X-ray Diffraction Studies. Single-crystal samples were cleaved from larger crystals and mounted onto cryoloops with Parabar oil. Single-crystal X-ray diffraction (SC-XRD) data were collected at room temperature on a Rigaku XtaLAB Synergy-S diffractometer equipped with a HyPix-6000HE Hybrid Photon Counting detector and Mo/Cu microfocus sealed X-ray sources. Mo Kα radiation was used (λ = 0.71073 Å). CrysalisPRO was used to process and integrate the data sets, and the structures were refined using Shelxle.[20,21] Direct methods were used to locate the lanthanide atoms, while positions of light atoms such as boron and carbon were found through the combined use of least-squares refinement and difference Fourier maps. All of the $Ln_3BC_2X_n$ compounds are structural analogues of $Ca_3C_3Cl_2$ (space group *Cmcm*) with the exception of $La_3BC_2Cl_2$, which is analogous to $La_3BC_2Br_2$ (space group *Pnma*).[22,23] Electron density peaks from interstitial hydride ions could not be observed; these hydrogen atoms were therefore positioned on the sites indicated by the neutron diffraction study of $La_3BC_2H_{1.7}$ (next section Neutron Diffraction Studies). Details of the crystallographic data for the X-ray diffraction studies are shown in Tables 1−3. Additional crystallographic data are available in the form of CIF files (see the Supporting Information).

Table 1. X-ray and Neutron Crystallographic Data and Collection Parameters for $Ln_3BC_2H_x$ with Hydride Interstitials

	$La_3BC_2H_{1.69}$ (neutron)	$Ce_3BC_2H_x$ (X-ray)	$Pr_3BC_2H_x$ (X-ray)
crystal system	orthorhombic		
space group	*Cmcm* (#63)		
a (Å)	3.805(2)	3.7404(6)	3.7076(2)
b (Å)	12.744(4)	12.436(2)	12.2653(5)
c (Å)	11.240(3)	11.1813(2)	11.1717(5)
volume (Å^3)	545.0(3)	520.2(2)	508.03(4)
Z	4		
index ranges	$-6 < h < 6; -22 < k < 22; -14 < l < 20$	$-4 < h < 4; -14 < k < 15; -12 < l < 14$	$-6 < h < 6; -20 < k < 20; -14 < l < 18$
reflections collected	5107	1487	2065
temperature	100	298	298
radiation	Neutron TOF	Mo K*α*	Mo K*α*
unique data/ parameters	931/33	398/22	754/21
μ (mm^{-1})	$0.0633 + 0.3509\lambda$	31.33	21.11
R1/wR2	0.0554/0.1102	0.0353/0.1300	0.0293/0.0717
R1/wR2 (all data)	0.0592/0.1116	0.0394/0.1325	0.0313/0.0730
max peak/ hole	1.71/−1.13 (fm/Å^3)	2.85/−2.41 (e-/Å^3)	3.64/−3.37 (e-/Å^3)

Neutron Diffraction Studies. Single-crystal neutron diffraction data were collected for the $La_3BC_2H_x$ analogue at 100 K using the TOPAZ diffractometer at Oak Ridge National Laboratory. A total of 14 crystal orientations were determined using the CrystalPlan software, which calculated optimal coverage for the symmetry of the unit cell.[24] To account for normal fluctuations in the output power of the neutron beam, each orientation was exposed to the neutron beam until it had collected 15 C of charge, which required about 3 h of exposure at a nominal neutron beam power of 1.4 MW. The integrated peak intensities were determined using the Mantid platform.[25] Data reduction (including detector efficiency, neutron TOF spectrum, and absorption corrections) was carried out using the ANVRED3 program.[26]

Magnetic Susceptibility and Electrical Transport Measurements. Magnetic susceptibility measurements were conducted on those products that yielded sufficiently large single crystals to detect possible magnetic ordering. Single crystals free of surface flux were selected and aligned on a piece of Kapton tape to position the long axis of the crystal (crystallographic *a*-axis) parallel to the applied field. This tape was then placed on a straw that was then attached to the sample rod of a Quantum Design MPMS SQUID system. Temperature dependence of magnetic susceptibility ($\chi = M/H$) data were collected from 1.8 to 300 K for $La_3BC_2H_{1.69}$ and $Pr_3BC_2H_x$ and from 15 to 300 K for $Ce_3BC_2H_x$ and $Pr_3BC_2F_{0.71}$. All measurements were done in an applied magnetic field of H = 2000 Oe. Additional measurements were carried on on the $La_3BC_2H_{1.69}$ compound at fields of H = 50 Oe and 5000 Oe. Electrical resistivity measurements were carried out on a single crystal of $La_3BC_2H_{1.69}$ with a four-wire configuration using a Quantum Design Physical Property Measurement System in the temperature range from 1.8 to 400 K and applied magnetic fields from 0 to 2 T.

Electronic Structure Calculations. The Stuttgart tight binding-linear muffin tin orbital-atomic sphere approximation (TB-LMTO-ASA) program package was used to calculate the density of states (DOS).[27] Calculations for $La_3BC_2H_{1.69}$ were performed based on unit cell parameters and atomic coordinates determined from neutron diffraction at 100 K. The neutron data indicate the tetrahedral interstitial site is fully occupied and the octahedral site is split and partially occupied. Therefore, calculations were carried out on two models: $La_2BC_2H_2$ (with both interstitial sites fully occupied, and the octahedral site centered/unsplit) and La_2BC_2H (with the tetrahedral site full and the octahedral site empty). For the fluorine analogues, a model based on $La_3BC_2F_{0.69}$ SC-XRD data collected at 296 K was used. For these, because both the tetrahedral and octahedral sites are partially occupied, two models $La_2BC_2F_2$ and La_2BC_2 were used, with the first model having both of its interstitial sites fully occupied and the second having both of its interstitial sites empty. The following basis sets were used: La (6s, 5d, 4f), C (2s, 2p), B (2s, 2p), and H(1s) or F(2s, 2p) (depending on the model), with La (6p), C (3d), and B (3d) being downfolded. Integration over the Brillouin zone was made by the tetrahedron method.[28]

RESULTS AND DISCUSSION

Synthesis. The compound $Ce_3BC_2H_x$ was initially found as a minor byproduct of a reaction of boron and anthracene in a Ce/Cu melt that produced $Ce_4B_2C_2H_{2.42}$, a hydride-stuffed variant of the Nd_2BC structure type in the monoclinic space group *C*2/*m*.[16] Both of these two phases form shiny, black, rod-shaped crystals that can be distinguished from each other only by single-crystal X-ray diffraction (see Figure 1). $Ce_3BC_2H_x$ was by far the minor product, making up approximately 10% of the crystals. The crystals range from 1 to 3 mm long and can grow up to about a quarter of a millimeter wide.

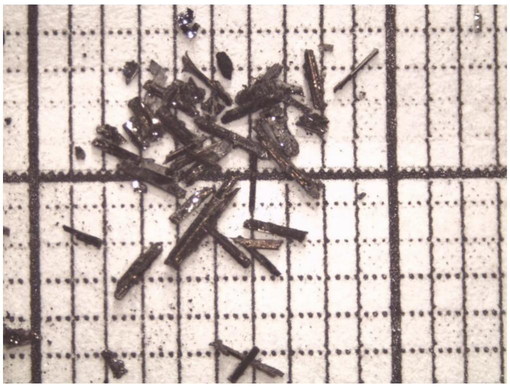

Figure 1. Microscope image of products of a reaction in Ce/Cu flux with a 1:1 mmol ratio of carbon and boron, showing a mixture of crystals of both orthorhombic $Ce_3BC_2H_x$ and monoclinic $Ce_4B_2C_2H_{2.42}$ on millimeter grid paper.

To modify the reaction to favor $Ce_3BC_2H_x$, the ratio of boron and anthracene reactants was changed to target the B:C ratio of 1:2 found in the desired product. In addition to optimizing the reactant ratios, the yield was also affected by the heating profile for the (Ce/Ni)/B/$C_{14}H_{10}$ reactions. Centrifuging immediately after cooling to 600 °C yielded small crystals with a large amount of powder. However, if the reaction mixture is allowed to sit at 600 °C, large crystals form, with no powder byproduct. These changes led to a nearly 100% yield of

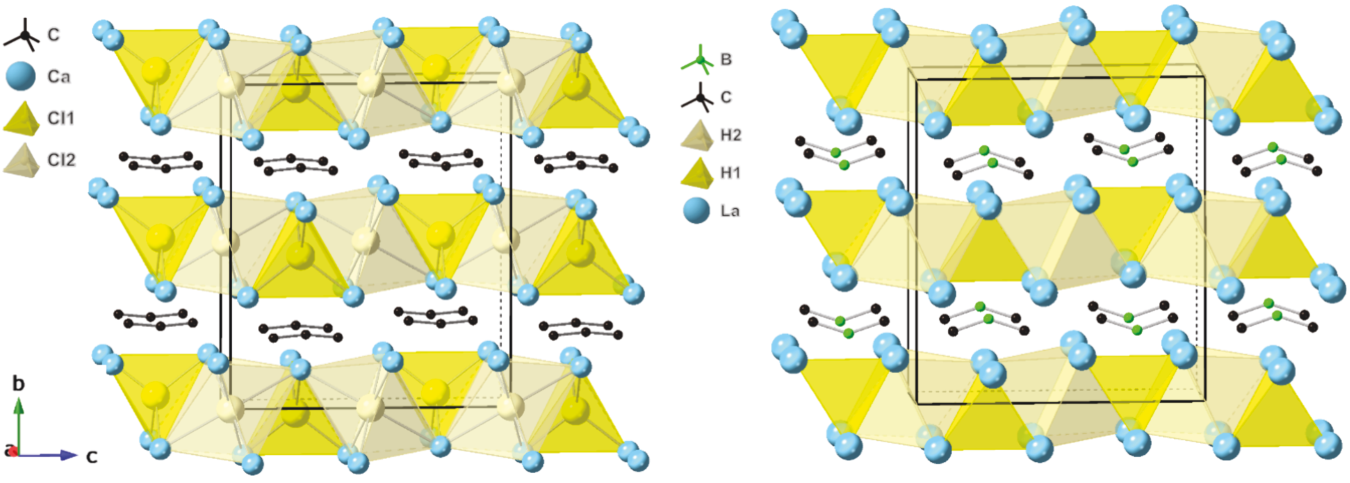

Figure 2. Structures of $Ca_3C_3Cl_2$ (*left*) and $Ce_3BC_2H_x$ (*right*) viewed down the *a*-axis. Interstitial atoms are shown in the polyhedral mode with tetrahedral positions in yellow and octahedral positions in pale yellow.

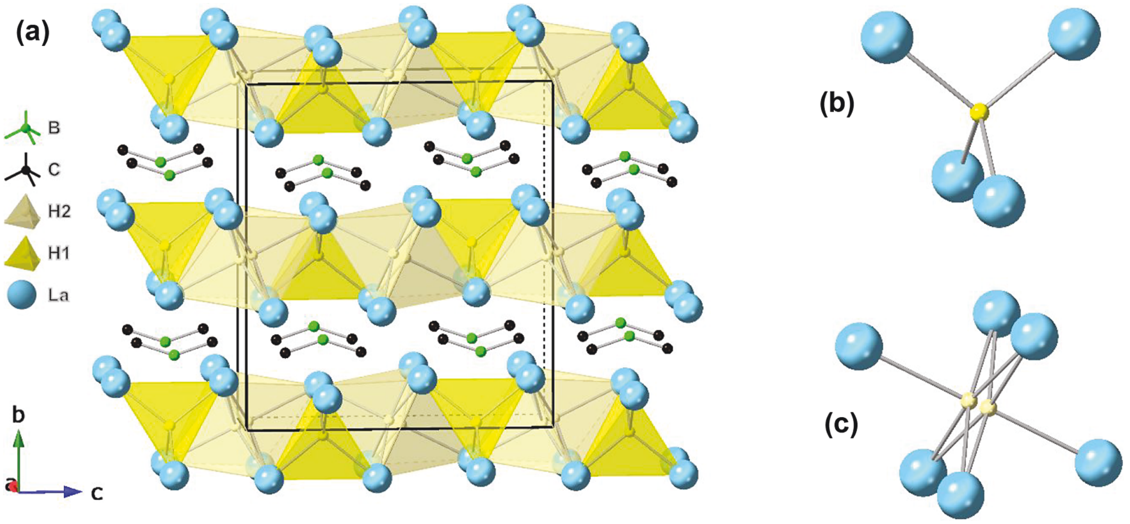

Figure 3. (a) Structure of $La_3BC_2H_{1.69}$ including hydride sites determined by neutron diffraction data, shown in the polyhedral mode. The tetrahedral site is colored yellow, and the octahedral site is colored pale yellow. (b) Local environment of the tetrahedral site. (c) Local environment of the octahedral site, showing the split hydride site.

the desired product. After $Ce_3BC_2H_x$ was grown with good yield, other lanthanide analogues were explored. $Ln_3BC_2H_x$ can be made with Ln = La, Ce, and Pr but cannot be formed with Ln = Nd, Sm, and Eu. Heavier lanthanides were not tried. It is likely that a size limit is reached with Nd.

Given the successful use of anthracene, we explored the use of decafluorobiphenyl ($C_{12}F_{10}$) as a source of both carbon and fluorine. $La_3BC_2F_{0.84}$ was made from a reaction of 0.2083 mmol of $C_{12}F_{10}$, 1 mmol of B, and 1.5 g of La/Ni flux. The same reaction with Ce and Pr would not yield any crystals. It was found that for these reactions, a small amount of anthracene was also needed to make the fluorinated analogues. For both of these reactions, a ratio of 0.0056 mmol of anthracene, 0.1601 mmol of decafluorobiphenyl, 1 mmol of B, and 1.5 g of either Ce/Ni or Pr/Ni flux was used. The amount of anthracene needed was determined experimentally, and yields of both of these products were low. The need for a small amount of anthracene suggests that the partially occupied fluoride interstitial sites are probably mixed hydride/fluoride sites in the cerium and praseodymium analogues of $Ln_3BC_2F_x$.

Structure of $Ln_3BC_2H_x$. $Ln_3BC_2H_x$ are analogues of $Ca_3C_3Cl_2$ with lanthanide cations in the calcium sites, a C−B−C chain instead of a C_3^{4-} allenylide unit, and, interestingly, "empty" chlorine sites (Figure 2).[19] The identification of the C−B−C chain was done by comparing the observed bond lengths to the C−B bond lengths in other similar structures. The carbon−boron bond in $Ce_3BC_2H_x$ is 1.51(1) Å, which is significantly longer than the C−C double bond found in allenylides (1.32−1.35 Å) and is well within the range of 1.48−1.52 Å found in other rare earth intermetallics with C−B−C chains.[22,23,29]

Given the formation of a structure analogous to that of $Ca_3C_3Cl_2$, we found it unlikely that the chloride sites were empty. If these sites are occupied, the lack of observable electron density on those positions in the SC-XRD refinement indicates that hydrogen is the most likely occupant. Hydrogen, with only one electron, does not diffract X-rays strongly enough compared to the surrounding lanthanide atoms to be visible with X-ray diffraction. Therefore, neutron diffraction data were collected on a single crystal of $La_3BC_2H_x$.

Neutron diffraction indicated the presence of hydrogen in both the tetrahedral and octahedral interstitial sites; see Figure 3. The tetrahedral site is fully occupied, with La−H distances of 2.472(4)−2.544(4) Å, which compare well to the 2.454 Å distance found in LaH_2.[30] The octahedral site is axially elongated. The hydride ion is not located in the center (a 4*c* Wyckoff site that would be 70% occupied); this site is instead split into two 8*f* Wyckoff sites, each 35(2)% occupied. The resulting La−H distances range from 2.747 to 2.887 Å. These are considerably longer than those found in LaH_2. The splitting of this hydrogen site likely serves to position the ion closer to one of the axial La positions, similar to the cause of the off-center titanium location in $BaTiO_3$. If hydrogen were in the middle of the octahedral site, the La−H axial distance would be 3.127 Å. The resulting overall stoichiometry is $La_3BC_2H_{1.69}$.

While neutron diffraction data were not available for the other $Ln_3BC_2H_x$ analogues (Ln = Ce, Pr), hydride interstitials are presumably present in these compounds as well, although their exact location and occupancy are not known. Placing hydrogen atoms in the center of the interstitial positions in $Ce_3BC_2H_x$ yields a Ce−H distance of 2.45 Å for the tetrahedral site and Ce−H distances ranging from 2.701 to 3.090 Å for the octahedral site. In the reported structure for CeH_3, the tetrahedral Ce−H distance is 2.4011(6) Å, while the octahedral Ce−H distance is 2.773(2) Å.[31] These values also compare well to the Ce−H distances indicated by neutron diffraction studies of $Ce_4B_2C_2H_{2.42}$, which has tetrahedral distances from 2.437 to 2.470 Å and octahedral Ce−H distances from 2.798 to 2.941 Å.[16] For the $Pr_3BC_2H_x$ analogue, the tetrahedral Pr−H distances are 2.406−2.535 Å and the octahedral Pr−H distances are 2.652−3.107 Å. The tetrahedral site matches well with the 2.389 Å distance reported for PrH_2.[30] Judging from the long (over 3 Å) axial Ln−H distance for the octahedral site in all of these structures, and the observed split site in $La_3BC_2H_{1.69}$, it is likely that this position is a split site in the other $Ln_3BC_2H_x$ analogues as well.

Structure of Fluoride Analogues. $Ln_3BC_2F_x$ analogues were made for all three Ln = La, Ce, and Pr. Incorporation of fluorine was confirmed by elemental analysis, and electron density peaks were observable with SC-XRD in both the tetrahedral and octahedral interstitial sites. In the La structure, the octahedral site was split as in $La_3BC_2H_{1.69}$; this site was *not* split in both the Ce and Pr analogues. Allowing the occupancy of the fluorine sites to vary gave the overall stoichiometries of $La_3BC_2F_{0.66}$, $Ce_3BC_2F_{0.59}$, and $Pr_3BC_2F_{0.71}$. The unit cell parameters are listed in Table 2. Comparing these to the unit cell parameters of the hydride analogues in Table 1, the unit cell volume of the La analogues increases from 545 to 563 $Å^3$ as hydrogen is replaced by fluorine. Conversely, the Ce and Pr fluoride analogues have unit cell parameters very similar to their corresponding hydrides. This may be explained by the likely mixing of hydride on these sites ($Ln_3BC_2F_x$ with Ln = Ce and Pr cannot be obtained without using both $C_{12}F_{10}$ and $C_{14}H_{10}$ reactants, indicating they are likely $Ln_3BC_2(F/H)_x$).

For $La_3BC_2F_{0.66}$, the occupancy of the tetrahedral site was found to be 33(3)%, while the octahedral position forms a split site that is 16(4)% occupied. The La−F distances for the tetrahedral site are 2.56(1) and 2.577(9) Å. The octahedral La−F distances were determined to be 2.60(3), 2.82(2), and 2.89(2) Å. The La−F distances in LaF_3 are 2.415−2.775 Å.[32] In the case of $Ce_3BC_2F_{0.59}$, the tetrahedral site was found to be 20(3)% occupied, and the octahedral site was found to be 39(4)% occupied. The Ce−F distances in the tetrahedral site were measured to be 2.42(1) and 2.56(2) Å, which compare well to those in CeF_3 (2.400−2.621 Å).[33] The octahedral Ce−F distances are longer (2.6941(1) and 3.134 Å). For $Pr_3BC_2F_{0.71}$, the tetrahedral site was found to be 19(3)% occupied and the octahedral site was 52(5)% occupied. The Pr−F distances in the tetrahedral site were measured to be 2.35(3) and 2.60(3) Å, in the range reported for PrF_3 (2.378−2.589 Å).[34] The Pr−F distances in the octahedral site are 2.6520(2) and 3.121(1) Å.

Table 2. X-ray Crystallographic Data and Collection Parameters for $Ln_3BC_2F_x$ with Fluoride Interstitials

	$La_3BC_2F_{0.66}$	$Ce_3BC_2F_{0.59}$	$Pr_3BC_2F_{0.71}$
crystal system	orthorhombic		
space group	*Cmcm* (#63)		
a (Å)	3.8189(3)	3.7267(2)	3.6928(3)
b (Å)	12.9822(1)	12.4893(8)	12.287(2)
c (Å)	11.3585(7)	11.1777(6)	11.1767(9)
volume ($Å^3$)	563.13(7)	520.25(5)	507.11(1)
Z	4		
index ranges	$-4 < h < 5$; $-16 < k < 16$; $-14 < l < 15$	$-5 < h < 5$; $-15 < k < 15$; $-12 < l < 13$	$-4 < h < 4$; $-15 < k < 16$; $-14 < l < 15$
reflections collected	2079	1492	4773
temperature (K)	295	200	297
radiation	Mo Kα		
unique data/ parameters	450/33	367/32	435/21
μ (mm^{-1})	22.20	25.65	28.20
R1/wR2	0.0271/0.0690	0.0212/0.0548	0.0563/0.1210
R1/wR2 (all data)	0.0275/0.0692	0.0215/0.0551	0.0926/0.1675
max peak/hole (e-/$Å^3$)	1.47/−1.67	1.88/−1.33	6.47/−3.26

Chloride Analogue and Structure Change. Attempts to make a chloride analogue of the above compounds from the reaction of boron, carbon, and $LaCl_3$ in La/Ni flux led to a low yield of $La_3BC_2Cl_x$. A slightly higher yield was obtained from the reaction in La/Fe flux. $La_3BC_2Cl_x$ forms as air-sensitive black crystals that are flat rods of up to 1 mm long and 0.25 mm wide. The total occupancy of the Cl sites varies across crystals with $0.17 < x < 1.01$. In the $La_3BC_2Cl_{1.01}$ product, the octahedral chlorine site is 85(6)% occupied. The La−Cl distances for that site are 3.0161(1) and 3.1819(1) Å. This distance is reasonable when compared to the La−Cl distances in the range of 2.835−2.993 Å for $LaCl_3$, $La_4Cl_5B_4$, and $La_5C_2Cl_9$.[35−37] The tetrahedral site is 17(8)% occupied. Its La−Cl distances are 2.58(7) and 2.67(7) Å, which are significantly shorter than those found in the literature. This may account for some of the electron density peaks consistently observed near the La sites in the single-crystal refinement as local distortions around the tetrahedral site may occur to move the La atoms further away from the chloride. The low yield, variable occupancy, and distortions in the structure point to the fact that chloride ions do not fit into the interstitial sites.

In accordance with this, increasing the amount of $LaCl_3$ reactant used (to achieve a 1:2:2 B/C/Cl reactant ratio) led to a change in the structure type; see Table 3. While the product had the desired $La_2BC_2Cl_2$ composition, it forms in the $La_3BC_2Br_2$ structure type (*Pnma*) instead of the $Ca_3C_3Cl_2$

Table 3. X-ray Crystallographic Data and Collection Parameters for $La_3BC_2Cl_{1.01}$ and $La_3BC_2Cl_2$

	$La_3BC_2Cl_{1.01}$	$La_3BC_2Cl_2$
crystal system	orthorhombic	
space group	*Cmcm* #63	*Pnma* #62
a (Å)	3.8409(1)	14.8700(6)
b (Å)	13.7068(3)	3.9011(2)
c (Å)	11.2820(2)	11.3704(5)
volume (Å^3)	593.96(2)	659.59(5)
Z	4	4
index ranges	$-10 < h < 9$; $-36 < k < 37$; $-30 < l < 26$	$-18 < h < 17$; $-4 < k < 5$; $-14 < l < 14$
reflections collected	19041	3578
temperature (K)	295	296
radiation	Mo Kα	
unique data/parameters	3455/31	924/49
μ (mm^{-1})	21.49	19.77
R1/wR2	0.0325/0.0821	0.0377/0.0894
R1/wR2 (all data)	0.0354/0.0835	0.0415/0.0927
Max peak/hole (e-/Å^3)	5.51/−8.89	2.24/−3.24

structure type (*Cmcm*) seen for the other $Ln_3BC_2X_n$ (X = H, F) compounds.[22,23] This $La_2BC_2Cl_2$ structure features the same repeating layers of La separated by layers of Cl atoms and layers of borocarbide anions as does $La_3BC_2Cl_{1.01}$; see Figure 4. However, the coordinations of the chloride anions are very different. In $La_3BC_2Cl_2$, the two unique chloride sites are both five-coordinate, in contrast to the octahedral and tetrahedral sites seen for $La_3BC_2Cl_{1.01}$. One is square pyramidal (with La−Cl distances ranging from 3.003(2) to 3.112(3) Å), and the other is trigonal bipyramidal (La−Cl distances from 3.067(2) to 3.283(3) Å). Because of the reduced symmetry of the space group, the $[C{-}B{-}C]^{7-}$ unit is asymmetrical, with the bond distance between C1 and B being 1.51(2) Å and the bond distance between C2 and the same B being 1.48(2) Å. The bond angle is 145(1)°. These distances and the angle lead to the assignment of a 7- charge. When combined with the full occupancy of the chlorine sites, this leads to a charge-balanced composition of $(La^{3+})_3[BC_2]^{7-}(Cl^-)_2$.

Electronic Structure Calculations. The calculated DOS data for $La_3BC_2H_{1.69}$ are shown in Figure 5. Because the octahedral site is partially occupied, two models were used to approximate the DOS. The first was calculated by setting both the tetrahedral and octahedral sites to be fully occupied, giving an overall stoichiometry of $La_3BC_2H_2$. The second model had the tetrahedral site filled with H and the octahedral site empty, giving La_3BC_2H. The DOS of $La_3BC_2H_2$ shows that it has a pseudogap at the Fermi level. On the other hand, the Fermi level for La_3BC_2H occurs at a peak in the DOS, which is somewhat destabilizing. Because the octahedral site of $La_3BC_2H_{1.69}$ is 35(3)% occupied and is a split site, the total occupancy of the site is 70%; therefore, the actual DOS is probably more similar to the $La_3BC_2H_2$ model. The hydride states are positioned between −1 and −3 eV below the Fermi level, in agreement with their anionic nature.

The DOS plots for $La_3BC_2F_x$ are shown in Figure 6. Because both interstitial sites are partially occupied by fluorine, two models were used to approximate the DOS for $La_3BC_2F_{0.66}$, the first being $La_3BC_2F_2$, with both interstitial sites being fully occupied, and the second being La_3BC_2, with both interstitial sites empty. The $La_3BC_2F_2$ model shows a distinct pseudogap at E_F, while the La_3BC_2 model shows the Fermi level positioned in a band of lanthanum states. Because both of the interstitial sites are less than 50% occupied, the actual DOS is probably closer to that of La_3BC_2, with some states at the Fermi level. The fluoride states are in a sharp narrow band at −5 eV below the E_F. This supports their anionic nature and their relative hardness compared to those of the corresponding hydride bands in Figure 5a. Both the hydride and fluoride compounds can shift from semimetallic (with a pseudogap at E_F) to metallic based on the filling of the interstitial sites, indicating that their transport properties can be tuned by controlling the incorporation of interstitial species.

Superconductivity of $La_3BC_2H_{1.69}$. The $La_3BC_2X_n$ compounds do not contain paramagnetic centers, so the contributions to magnetic behavior are expected to be the core

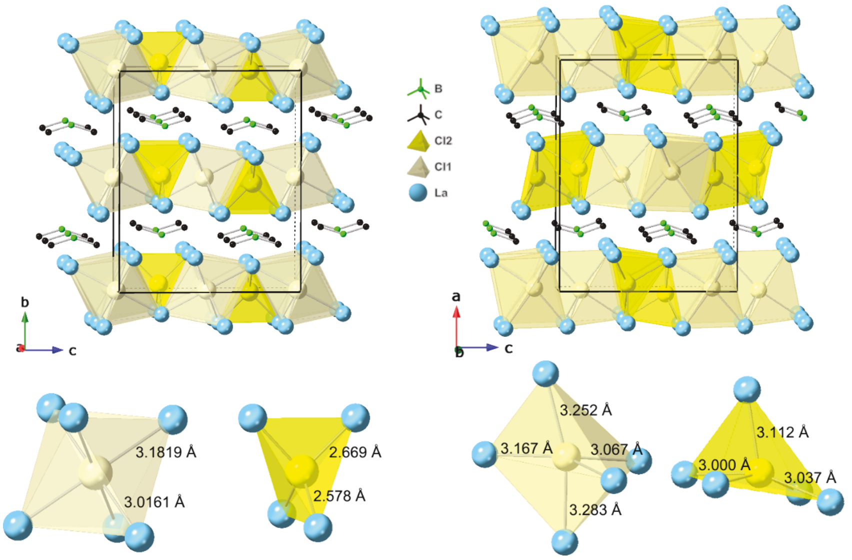

Figure 4. Comparison of the structures of $La_3BC_2Cl_{1.01}$ ($Ca_3C_3Cl_2$ type in *Cmcm*, left) and $La_3BC_2Cl_2$ ($La_3BC_2Br_2$ type in *Pnma*, right). Chloride sites are shown in the polyhedral mode, with representative bond lengths.

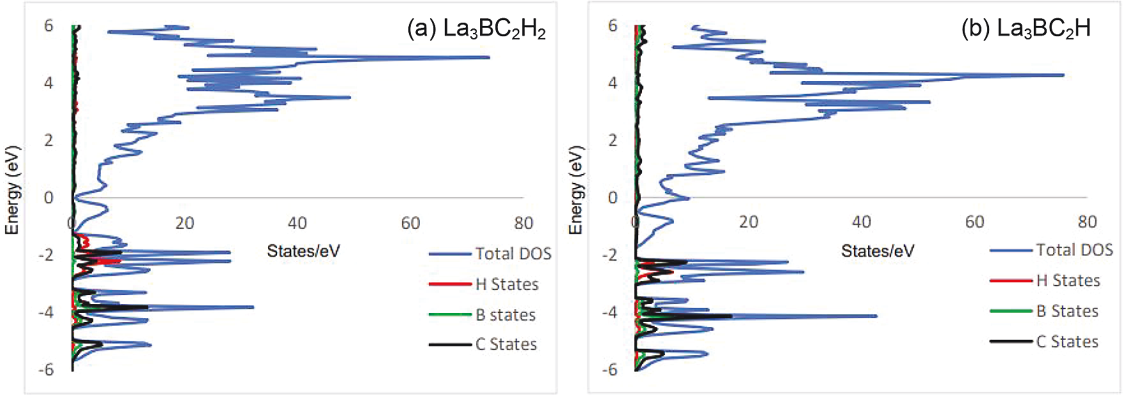

Figure 5. (a) Total and partial DOS data calculated for $La_3BC_2H_2$, with both interstitial sites fully occupied. (b) DOS for La_3BC_2H, with only tetrahedral sites occupied. The Fermi level is set to 0 eV.

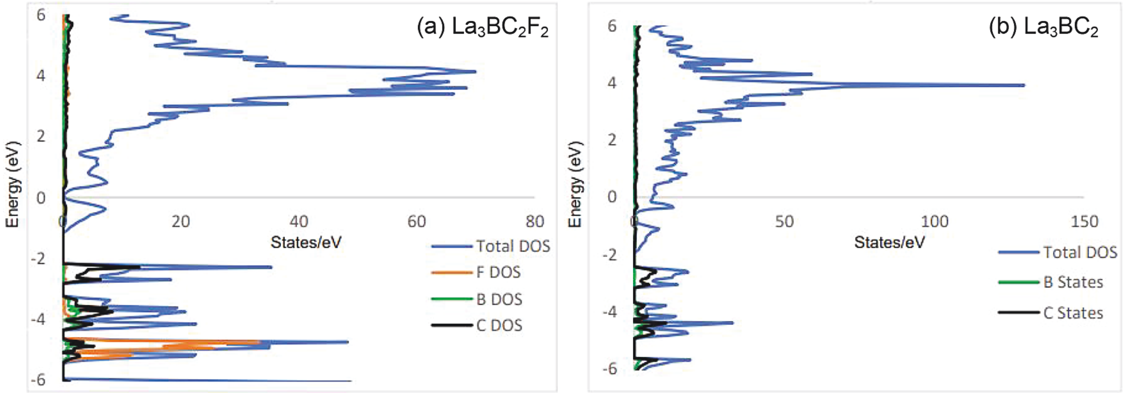

Figure 6. (a) DOS calculated for $La_3BC_2F_2$ with both interstitial sites fully occupied. (b) DOS for La_3BC_2 with both interstitial sites empty. The Fermi level is set to 0 eV.

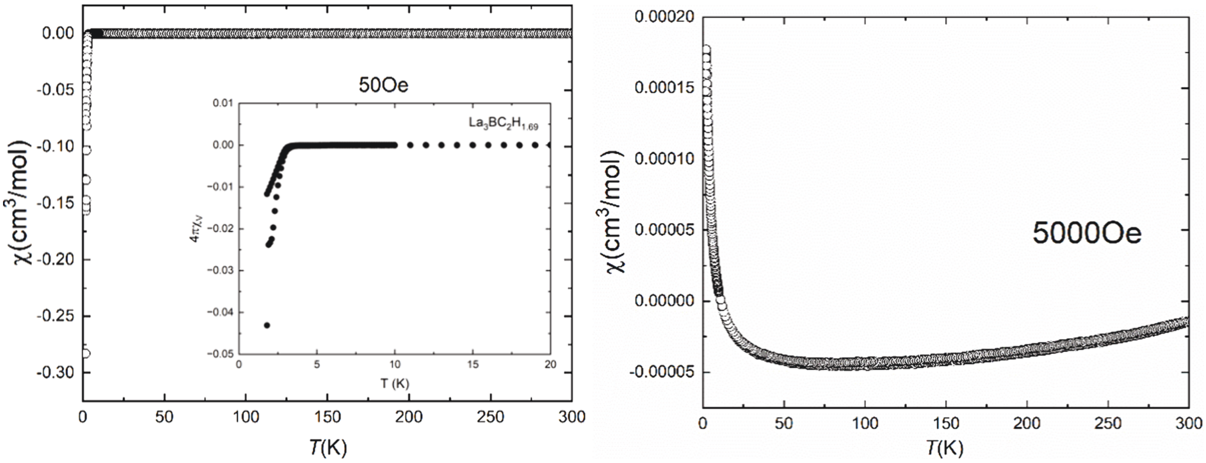

Figure 7. Magnetic susceptibility data for $La_3BC_2H_{1.67}$ collected at applied fields of 50 (left; inset shows volume susceptibility and FC/ZFC splitting below T_C) and 5000 Oe (right).

diamagnetism of the lanthanum ions and the Pauli paramagnetism of the conduction electrons. Magnetic susceptibility data were collected on the hydride analogue $La_3BC_2H_{1.69}$ at 50 and 5000 Oe (shown in Figure 7). Both show very low diamagnetism at high temperatures, indicating that the core diamagnetism outweighs the contribution from conduction electrons. This is another indication that this compound is a poor metal or semimetal with a low DOS at the Fermi level (Figure 5a). For the data collected at the lower applied field, a sharp drop in the susceptibility occurs below 3.2 K, indicating that the compound becomes superconducting. This is reproducible in several samples. Splitting of field-cooled and zero-field-cooled behaviors at T_C is observed. However, calculation of the volume susceptibility (Figure 7, inset) indicates that the superconducting fraction is below 5%. Since the data were collected on single crystals, this is unlikely to be caused by an impurity or secondary phase, but instead is caused by regions of inhomogeneous hydride content in the samples.

Resistivity measurements were carried out on a single crystal of $La_3BC_2H_{1.67}$ at varying fields; the data are shown in Figure 8.

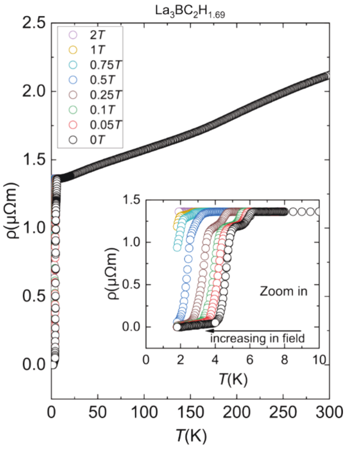

Figure 8. Resistivity measurements on a single crystal of $La_3BC_2H_{1.69}$ at different fields. The data near the transition are highlighted in the inset.

In the normal state, this compound behaves like a poor metal, with resistivity on the order of 1 $\mu\Omega\cdot m$ (similar to bismuth) that rises with temperature. The transition to a superconducting state is observed below 5 K. The transition temperature decreases with increasing field strength; the T_C is about 4.5 K at 0 T and falls below 2.5 K at a field of 0.5 T. It is notable that this transition exhibits two steps. This may be due to the inherently disordered structure caused by partial occupancy of the hydride in the octahedral interstitial sites. The material may have small regions of $La_3BC_2H_2$ (with both tetrahedral and interstitial sites fully occupied) that have a higher T_C that produces the higher temperature transition, while other regions of the crystal (with partial occupancy of the octahedral sites) transition to the superconducting state at a slightly lower temperature. A similar stepped behavior due to inhomogeneity was seen in the superconducting transition of $BaPb_{1-x}Bi_xO_3$.[38] This is also in agreement with the low superconducting fraction indicated by the magnetic susceptibility data in Figure 7. While diffraction indicates an average stoichiometry of $La_3BC_2H_{1.7}$, small regions of the sample with a specific amount of hydride x ($La_3BC_2H_x$) become superconducting, while regions with different hydride contents do not. This is akin to what is observed in LaFePO, which has a low superconducting fraction that is caused by the presence of oxygen defects at/near the surface of the crystals.[39] Exploration of the effect of varying the interstitial occupancies of $La_3BC_2H_x$ is underway along with annealing experiments to promote uniform distribution of the hydrides. The crystals of the fluoride and chloride analogues were too small for resistivity and magnetic susceptibility measurements.

Magnetic Susceptibility of $Ln_3BC_2X_n$ (Ln = Ce, Pr). The Ln = Ce or Pr analogues contain lanthanides with localized *f*-electrons and are therefore expected to be paramagnetic. Preliminary magnetic susceptibility data for $Ce_3BC_2H_x$ (Figure 9) show no magnetic transition down to low temperatures; above 100 K, the data can be fitted to the Curie−Weiss law. The resulting magnetic moment per Ce^{3+} and the Weiss constant are 2.62 μ_B and −23.2 K, respectively. The magnetic moment is close to the theoretical value expected for Ce^{3+} (2.54 μ_B). We were unable to obtain crystals of $Ce_3BC_2F_{0.59}$ large enough for magnetic measurements to compare to those of the hydride analogue.

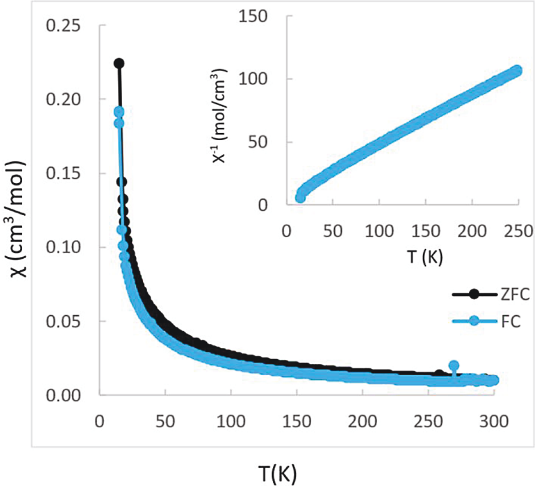

Figure 9. Temperature-dependent magnetic susceptibility of $Ce_3BC_2H_x$ collected at 2000 Oe. ZFC is shown in black, and FC is shown in blue. Inset: Inverse susceptibility data $1/\chi$.

Magnetic susceptibility data for both $Pr_3BC_2H_x$ and $Pr_3BC_2F_{0.71}$ are shown in Figure 10. $Pr_3BC_2H_x$ shows ferromagnetic ordering at around 55 K along with significant ZFC-FC splitting at the same temperature. A subsequent drop in the ZFC susceptibility below 35 K may indicate that a spin reorientation to an antiferromagnetic configuration is occurring; further data including isothermal field-dependence studies are needed to investigate this, which will be the topic of future work. The data above 100 K (in the paramagnetic state) was fit to the Curie−Weiss equation, and the magnetic moment per Pr^{3+} was found to be 3.58 μ_B, which matches the expected value. The Weiss constant was calculated to be −2.14 K. These data indicate competing magnetic coupling forces are present between the two crystallographically unique Pr^{3+} sites.

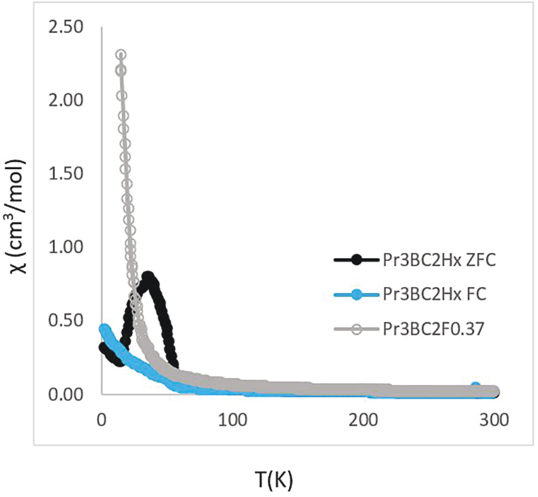

Figure 10. Temperature-dependent magnetic susceptibility of $Pr_3BC_2H_x$ and $Pr_3BC_2F_{0.71}$ collected at 2000 Oe. ZFC for $Pr_3BC_2H_x$ is shown in black, FC for $Pr_3BC_2H_x$ is shown in blue, and both ZFC and FC for $Pr_3BC_2F_{0.71}$ are shown in gray.

A weak antiferromagnetic coupling force is slightly prevalent at high temperatures (indicated by the negative Weiss constant), but ferromagnetic ordering at 55 K followed by a spin reorientation indicates ferromagnetic coupling is also present.

The fluorine analogue $Pr_3BC_2F_{0.71}$ shows a very different behavior. The magnetic susceptibility shows no magnetic ordering down to low temperatures. The distinct difference in magnetic behavior on going from the hydride to the fluoride indicates that magnetic coupling between Pr^{3+} ions can be drastically changed by varying the identity and the occupancy of interstitial ions. As mentioned previously, the fluoride analogue likely also contains hydride interstitials since it cannot be grown in the absence of anthracene (a source of hydride). This elimination of magnetic ordering upon going from $Pr_3BC_2H_x$ to $Pr_3BC_2(H/F)_x$ may be due to the increased disorder in the compound produced by the H/F site mixing, which will hinder/destroy long-range magnetic coupling forces. This is akin to the behavior observed in the previously reported $Ce_4B_2C_2H_{2.4}$ and $Ce_4B_2C_2H_{2.2}F_{0.4}$ systems; the former exhibits an antiferromagnetic ordering transition at 7 K, which is not seen for the latter analogue. The hydride positions and H/F mixing in the interstitial sites of those compounds were confirmed by neutron diffraction.[16,18]

CONCLUSIONS

New $La_3BC_2H_{1.69}$, $Ce_3BC_2H_x$, and $Pr_3BC_2H_x$ structures have been made by reacting the Ln/Ni flux with boron and anthracene. Their fluoride analogues $Ln_3BC_2F_x$ have also been made by using decafluorobiphenyl as the carbon and fluorine source. These structures share a structure type with $Ca_3C_3Cl_2$, which can be viewed as lanthanide borocarbide slabs separated by layers that can incorporate interstitials. This family of materials indicates the importance of interstitial chemistry; slight modifications of the hydride content or element mixing can have a dramatic effect on properties. The superconducting transition of $La_3BC_2H_x$ is likely dependent on the amount of hydride interstitials, as is also reported for PdH_x.[40] Efforts are underway to control the amount and homogeneous distribution of interstitials and also to make a deuterated analogue of $La_3BC_2H_{1.69}$. Since substitution of fluoride for hydride has a dramatic effect on magnetic properties, we are also attempting the growth of larger crystals of the $La_3BC_2F_x$ analogue as well as $La_3BC_2(H/F)_x$ analogues to observe effects on the superconducting transition.

ASSOCIATED CONTENT

Supporting Information

The Supporting Information is available free of charge at https://pubs.acs.org/doi/10.1021/acs.chemmater.4c02111.

$Ln_3BC_2X_n$ combined REV (CIF)

AUTHOR INFORMATION

Corresponding Author

Susan E. Latturner − *Department of Chemistry and Biochemistry, Florida State University, Tallahassee, Florida 32306, United States;* orcid.org/0000-0002-6146-5333; Email: slatturner@fsu.edu

Authors

James T. Larson − *Department of Chemistry and Biochemistry, Florida State University, Tallahassee, Florida 32306, United States*

Katelyn Wix − *Department of Chemistry and Biochemistry, Florida State University, Tallahassee, Florida 32306, United States*

Olatunde Oladehin − *Department of Physics and National High Magnetic Field Laboratory, Tallahassee, Florida 32310, United States*

Ryan Baumbach − *Department of Physics and National High Magnetic Field Laboratory, Tallahassee, Florida 32310, United States*

Xiaoping Wang − *Neutron Scattering Division, Oak Ridge National Laboratory, Oak Ridge, Tennessee 37831, United States;* orcid.org/0000-0001-7143-8112

Complete contact information is available at: https://pubs.acs.org/10.1021/acs.chemmater.4c02111

Notes

The authors declare no competing financial interest.

ACKNOWLEDGMENTS

This project was supported by the National Science Foundation Division of Materials Research (DMR-2126077). This work used the X-ray Characterization Center in the FSU Department of Chemistry and Biochemistry (FSU075000X-RAY), as well as the Scanning Electron Microscope in the Biological Sciences Imaging Resource (BSIR) of the FSU Department of Biology. Single-crystal neutron diffraction data were collected using the TOPAZ instrument (BL-12) at the Spallation Neutron Source, a DOE Office of Science User Facility operated by the Oak Ridge National Laboratory.

REFERENCES

(1) Phelan, W. A.; Menard, M. C.; Kangas, M. J.; McCandless, G. T.; Drake, B. L.; Chan, J. Y. Adventures in Crystal Growth: Synthesis and Characterization of Single Crystals of Complex Intermetallic Compounds. *Chem. Mater.* **2012**, *24*, 409−420.

(2) Du, X.; Graedel, T. E. Global Rare Earth In-Use Stocks in NdFeB Permanent Magnets. *J. Indust. Ecol.* **2011**, *15*, 836−843.

(3) Yamaguchi, M.; Inui, H.; Ito, K. High-temperature structural Intermetallics. *Acta Mater.* **2000**, *48*, 307−322.

(4) Cava, R. J.; Takagi, H.; Zandbergen, H. W.; Krajewski, J. J.; Peck, W. F.; Siegrist, T.; Batlogg, B.; van Dover, R. B.; Felder, R. J.; Mizuhashi, K.; Lee, J. O.; Eisaki, H.; Uchida, S. Superconductivity in the quaternary intermetallic compounds $LnNi_2B_2C$. *Nature* **1994**, *367*, 252−253.

(5) Nagamatsu, J.; Nakagawa, N.; Muranaka, T.; Zenitani, Y.; Akimitsu, J. Superconductivity at 39 K in magnesium diboride. *Nature* **2001**, *410*, 63−64.

(6) Buschow, K. H. J.; Sherwood, R. C. Magnetic properties and hydrogen absorption in rare-earth Intermetallics of the type RMn_2 and R_6Mn_{23}. *J. Appl. Phys.* **1977**, *48*, 4643−4648.

(7) Drozdov, A. P.; Kong, P. P.; Minkov, V. S.; Besediin, S. P.; Kuzovnikov, M. A.; Mozaffari, S.; Balicas, L.; Balakirev, F. F.; Graf, D. E.; Prakapenka, V. B.; Greenberg, E.; Knyazev, D. A.; Tkacz, M.; Eremets, M. I. Superconductivity at 250 K in lanthanum hydride under high pressures. *Nature* **2019**, *569*, 528−531.

(8) Kanatzidis, M. G.; Pöttgen, R.; Jeitschko, W. The Metal Flux: A Preparative Tool for the Exploration of Intermetallic Compounds. *Angew. Chem., Int. Ed.* **2005**, *44*, 6996−7023.

(9) Canfield, P. C.; Fisher, I. R. High-temperature solution growth of intermetallic single crystals and quasicrystals. *J. Cryst. Growth* **2001**, *225*, 155−161.

(10) Simon, A.; Babizhetskyy, V.; Oeckler, O.; Mattausch, H. J.; Bauer, J.; Kremer, R. K. Crystal Structure and Real Structure Investigations on the Intermittent Superconductivity of "$La_5B_2C_6$". *Z. Anorg. Allg. Chem.* **2005**, *631*, 316−326.

(11) Babizhetskyy, V.; Simon, A.; Bauer, J. Interaction of Lanthanum with Boron and Carbon: Phase Diagram and Structural Chemistry. *Monatsh. Chem.* **2014**, *145*, 869−876.

(12) Benbow, E. M.; Dalal, N. S.; Latturner, S. E. Spin glass behavior of isolated, geometrically frustrated tetrahedra of iron atoms in the intermetallic $La_{21}Fe_8Sn_7C_{12}$. *J. Am. Chem. Soc.* **2009**, *131*, 3349−3354.

(13) Jayasinghe, A. S.; Latturner, S. E. Metal Flux Growth of Praseodymium Iron Carbides Featuring FeC_3 Units. *Cryst. Growth & Design* **2021**, *21*, 103−111.

(14) Tucker, P. C.; Nyffeler, J.; Chen, B.; Ozarowski, A.; Stillwell, R.; Latturner, S. E. A Tale of Two Metals: New Cerium Iron Borocarbide Intermetallics Grown from Rare-Earth/Transition Metal Eutectic Fluxes. *J. Am. Chem. Soc.* **2012**, *134*, 12138−12148.

(15) Engstrand, T. O.; Cope, E. M.; Vasquez, G.; Haddock, J. W.; Hertz, M. B.; Wang, X.; Latturner, S. E. Flux synthesis of a metal carbide hydride using anthracene as a reactant. *Inorg. Chem.* **2020**, *59*, 11651−11657.

(16) Hertz, M. B.; Baumbach, R.; Wang, X.; Latturner, S. E. Unexpected Hydride: $Ce_4B_2C_2H_{2.42}$, a Stuffed Variant of the Nd_2BC Structure Type. *Cryst. Growth & Design* **2021**, *21*, 5164−5171.

(17) Larson, J. T.; Latturner, S. E. Flux growth of an intermetallic with interstitial fluorides via decomposition of a fluorocarbon. *Inorg. Chem.* **2023**, *62*, 1508−1512.

(18) Larson, J. T.; Hoffmann, C.; Latturner, S. E. $Ce_4B_2C_2F_{0.14}H_{2.26}$: Cerium borocarbides with fluoride and hydride interstitials grown from Ce/Cu flux. *Cryst. Growth Des.* **2023**, *23*, 5919−5924.

(19) Meyer, H.-J. Darstellung und Kristallstruktur eines Calciumcarbidchlorides mit einer C_3^{4-}-Einheit, $Ca_3Cl_2C_3$. *Z. Anorg. Allg. Chem.* **1991**, *593*, 185−192.

(20) CrysAlisPRO; Oxford Diffraction/Agilent Technologies UK Ltd: Yarnton, England.

(21) Hubschle, C. B.; Sheldrick, G. M.; Dittrich, B. ShelXle: a Qt graphical user interface for SHELXL. *J. Appl. Crystallogr.* **2011**, *44*, 1281−1284.

(22) Mattausch, H.; Oeckler, O.; Simon, A. B and B−C as interstitials in reduced rare earth halides. *Inorg. Chim. Acta* **1999**, *289*, 174−190.

(23) Mattausch, H.; Simon, A. Bromides of Rare Earth Metal Boride Carbides–A System of Building Blocks. *Angew. Chem., Int. Ed.* **1995**, *34*, 1633−1636.

(24) Zikovsky, J.; Peterson, P. F.; Wang, X. P.; Frost, M.; Hoffmann, C. CrystalPlan: an experiment-planning tool for crystallography. *J. Appl. Crystallogr.* **2011**, *44*, 418−423.

(25) Arnold, O.; Bilheux, J. C.; Borreguero, J. M.; Buts, A.; Campbell, S. I.; Chapon, L.; Doucet, M.; Draper, N.; Ferraz Leal, R.; Gigg, M. A.; et al. Mantid—Data analysis and visualization package for neutron scattering and μ SR experiments. *Nuclear Instruments and Methods in Physics Research Section A: Accelerators, Spectrometers, Detectors and Associated Equipment* **2014**, *764*, 156−166.

(26) Schultz, A. J.; Jørgensen, M. R. V.; Wang, X.; Mikkelson, R. L.; Mikkelson, D. J.; Lynch, V. E.; Peterson, P. F.; Green, M. L.; Hoffmann, C. M. Integration of neutron time-of-flight single-crystal Bragg peaks in reciprocal space. *J. Appl. Crystallogr.* **2014**, *47*, 915−921.

(27) Tank, R.; Jepsen, O.; Burkhardt, A.; Andersen, O. *The TB-LMTO-ASA Program*, 1994.

(28) Blöchl, P. E.; Jepsen, O.; Andersen, O. K. Improved tetrahedron method for Brillouin-zone integrations. *Phys. Rev. B* **1994**, *49*, 16223−16233.

(29) Lang, D. A.; Zaikina, J. V.; Lovingood, D. D.; Gedris, T. E.; Latturner, S. E. Ca_2LiC_3H: A New Complex Carbide Hydride Phase Grown in Metal Flux. *J. Am. Chem. Soc.* **2010**, *132*, 17523−17530.

(30) Holley, C. E., Jr.; Mulford, R. N. R.; Ellinger, F. H.; Koehier, W. C.; Zachariasen, W. H. The Crystal Structure of Some Rare Earth Hydrides. *J. Phys. Chem.* **1955**, *59*, 1226−1228.

(31) Korst, W. L.; Warf, J. C. Rare Earth-Hydrogen Systems. I. Structural and Thermodynamic Properties. *Inorg. Chem.* **1966**, *5*, 1719−1726.

(32) Zalkin, A.; Templeton, D. H.; Hopkins, T. E. The Atomic Parameters in the Lanthanum Trifluoride Structure. *Inorg. Chem.* **1966**, *5*, 1466−1468.

(33) Cheetham, A. K.; Fender, B. E. F.; Fuess, H.; Wright, A. F. A powder neutron diffraction study of lanthanum and cerium trifluorides. *Acta Cryst. Section B* **1976**, *32*, 94−97.

(34) From Cambridge University Press Cambridge Core. Greis, O.; Ziel, R.; Breidenstein, B.; Haase, A.; Petzel, T. Structural data of the tysonite-type superstructure modification β-PrF_3 from X-ray powder and electron single-crystal diffraction. *Powder Diffraction* **1995**, *10*, 44−46.

(35) Morosin, B. Crystal Structures of Anhydrous Rare-earth Chlorides. *J. Chem. Phys.* **1968**, *49*, 3007−3012.

(36) Mattausch, H. J.; Oeckler, O.; Simon, A. Rare Earth Halides Ln_4X_5Z. Part 3: The Chloride $La_4Cl_5B_4$−Preparation, Structure, and Relation to $La_4Br_5B_4$, $La_4I_5B_4$. *Z. Anorg. Allg. Chem.* **2008**, *634*, 503−506.

(37) Uhrlandt, S.; Heuer, T.; Meyer, G. Ternare Chloride mit trigonal-bipyramidalen clustern: $[M_5(C_2)]Cl_9$ (M = La-Pr). *Z. Anorg. Allg. Chem.* **1995**, *621*, 1299−1303.

(38) Giraldo-Gallo, P.; Lee, H.; Beasley, M. R.; Geballe, T. H.; Fisher, I. R. Inhomogeneous Superconductivity in $BaPb_{1-x}Bi_xO_3$. *J. Supercond. Nov. Magn.* **2013**, *26*, 2675−2678.

(39) Hamlin, J. J.; Baumbach, R. E.; Zocco, D. A.; Sayles, T. A.; Maple, M. B. Superconductivity in single crystals of LaFePO. *J. Phys.: Condens. Matter* **2008**, *20*, 365220.

(40) Kawae, T.; Inagaki, Y.; Wen, S.; Hirota, S.; Itou, D.; Kimura, T. Superconductivity in Palladium Hydride Systems. *J. Phys. Soc. Jpn.* **2020**, *89*, No. 051004.